PERGAMON

International Journal of Solids and Structures 38 (2001) 1641–1655

INTERNATIONAL JOURNAL OF SOLIDS and STRUCTURES

www.elsevier.com/locate/ijsolstr

Active control of FGM plates with integrated piezoelectric sensors and actuators

X.Q. He [a], T.Y. Ng [b], S. Sivashanker [a], K.M. Liew [a,*]

[a] *Centre for Advanced Numerical Engineering Simulations, School of Mechanical and Production Engineering, Nanyang Technological University, Nanyang Avenue, Singapore 639798, Singapore*

[b] *Institute of High Performance Computing, 89B Science Park Drive, #02-11/12, The Rutherford, Singapore 118261, Singapore*

Received 9 February 2000

Abstract

In this paper, a finite element formulation based on the classical laminated plate theory is presented for the shape and vibration control of the functionally graded material (FGM) plates with integrated piezoelectric sensors and actuators. The properties of the FGM plates are functionally graded in the thickness direction according to a volume fraction power law distribution. A constant velocity feedback control algorithm is used for the active control of the dynamic response of the FGM plate through closed loop control. The static and dynamic responses are presented in both tabular and graphical forms for an FGM plate of aluminum oxide/Ti–6A1–4V material composition. The effects of the constituent volume fractions and the influence of feedback control gain on the static and dynamic responses of FGM plates are examined.

Keywords: Functionally graded material composites; Sensor/actuator layers; Finite element method; Active deflection/vibration control

1. Introduction

The use of piezoelectric sensor and actuator systems for the active vibration suppression and shape control is fast becoming an essential tool in the design of smart structures and systems. The piezoelectric sensor is able to respond to the vibrations and generate a voltage due to the direct piezoelectric effect. This voltage is processed and amplified by a feedback gain and then applied onto an actuator. The actuator in turn produces a control force due to the converse piezoelectric effect. If the control force is appropriate, the vibration of the structure may be suppressed adequately.

Thus far, studies on the analysis of smart structures with surface or embedded piezoelectric sensors and actuators have focused mainly on the analytical techniques of Plump et al. (1987), Crawley and de Luis (1987), Lee et al. (1991) and Lam and Ng (1999). The major drawback of using an analytical approach is that it can only be used for a limited variety of simple structures such as beams or simply supported plates.

* Corresponding author. Tel.: +65-790-4076; fax: +65-793-6763.
E-mail address: mkmliew@ntu.edu.sg (K.M. Liew).

0020-7683/01/$ - see front matter
PII: S0020-7683(00)00050-0

For more complicated structures with integrated piezoelectric materials, finite element analysis may be required. Early investigations into the finite element formulation for piezoelectric solids were conducted by Allik and Hughes (1970). The interaction between electricity and elasticity were analyzed using tetrahedral elements. However, these elements were too thick for thin shell or plate applications. To overcome this drawback, Tzou and Tseng (1990) proposed a "thin" piezoelectric solid element by adding three internal degrees of freedom for the vibration control of structures with piezoelectric materials. Hwang et al. (1993) employed classical laminated plate theory (CLPT) to analyze the vibration control of a laminated plate with piezoelectric sensors and actuators. Their study explored the optimal design of the piezoelectric sensors and actuators. Based on the first-order shear deformation theory, Chandrashekhare and Tenneti (1995) developed a finite element model for the vibration control of laminated plates with piezoelectric sensors and actuators and analyzed the thermally induced vibration suppression of laminated plates. Robbins and Reddy (1991) presented the finite element model of a piezoelectrically actuated beam by using four different displacement-based one-dimensional beam theories all of which can be reduced from the generalized laminated plate theory of Reddy (1987). The static and dynamic interactions between a bonded piezoelectric actuator and an underlying beam substructure were investigated in this work. A number of approaches have been introduced to model the laminated shells containing piezoelectric layers. Based on the shear elastic shell theory of the Reissner–Mindlin type, Lammering (1991) developed a finite element model for the vibration control of a shell structure with piezoelectric layers. By using the direct method of Lyapunov, a control law is derived for the vibration control and asymptotic stability. Further, Heyliger et al. (1996) constructed a finite element model for laminated piezoelectric shells using a discrete-layer theory that allows for the discontinuous shear strain through the shell thickness. The active and sensory response of a cylindrical ring was studied.

Additionally, a relatively new class of composite materials known as "functionally graded materials" (FGMs) first developed by the Japanese in the late 1980s is characterized by the smooth and continuous change of the mechanical properties from one surface to the other, Yamanouchi et al. (1990). Due to its superior thermo-mechanical properties, FGMs have found extensive applications in various industries. Substantial research work have been done on the FGMs, Williamson et al. (1993), Obata and Noda (1996), and Praveen and Reddy (1998). However, to the authors' knowledge, minimal or no work has been presented in the literature for the active control of FGM structures using piezoelectric materials.

In this study, a finite element model based on CLPT is presented for the shape and vibration control analysis of the FGM plates with piezoelectric sensors and actuators. The constant velocity feedback control algorithm is used in a closed control loop. The shape control and vibration suppression of the FGM plates is performed to show the effectiveness of the presently developed finite element model with piezoelectric integration. The influence of the constituent volume fractions of Ti–6A1–4V is also studied for the static deflection, natural frequency and dynamic response of the FGM plates.

2. Analytical model

Consider an FGM plate with the integrated sensors and actuators as shown in Fig. 1. The top layer of the laminated plate is the piezoelectric actuator layer and the bottom layer is the piezoelectric sensing layer. The intermediate layer is an FGM plate that is made of the combined aluminum oxide and Ti–6A1–4V materials, and its properties are graded through the thickness direction according to a volume fraction power law distribution. Functionally gradient materials are mainly used in high temperature environments, and the constituent materials possess temperature-dependent properties. The material properties can be expressed as follows (Touloukian, 1967):

$$P = P_0(P_{-1}T^{-1} + 1 + P_1T + P_2T^2 + P_3T^3), \tag{1}$$

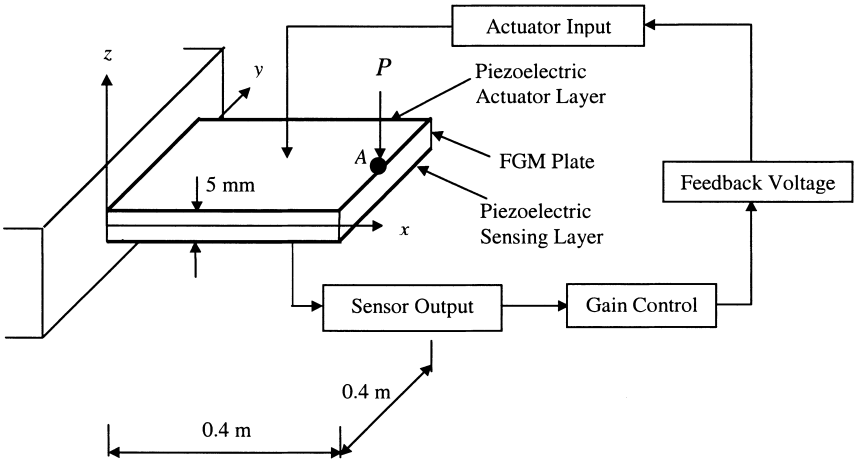

Fig. 1. Schematic diagram showing the feedback configuration of the FGM plate with piezoelectric sensor/actuator layers.

where P_0, P_{-1}, P_1, P_2 and P_3 are the coefficients of temperature T. Since the FGM considered here is a mixture of two materials, the effective properties which are both temperature and position dependent, can be expressed as

$$P_{\text{eff}}(T,z) = P_T(T)V_T(z) + P_{\text{A}}(T)(1 - V_T(z)), \tag{2}$$

where P_{eff} is the effective material property of the functionally gradient material, and P_T and P_{A} are the temperature dependent properties of the Ti–6A1–4V and aluminum oxide, respectively. V_T is the volume fraction of the Ti–6A1–4V constituent of the FGM and can be written as

$$V_T = \left(\frac{2z+h}{2h}\right)^n, \tag{3}$$

where n is the volume fraction exponent $(0 \leqslant n \leqslant \infty)$.

3. Theoretical formulation using classical laminated plate theory

3.1. Displacements and strains

The formulation presented here is based on the classical laminated plate theory (CLPT), which leads to the following displacement field:

$$\{u\} = \begin{Bmatrix} u_1 \\ u_2 \\ u_3 \end{Bmatrix} = \begin{Bmatrix} u_0 \\ v_0 \\ w_0 \end{Bmatrix} - \begin{Bmatrix} z\frac{\partial w_0}{\partial x} \\ z\frac{\partial w_0}{\partial y} \\ 0 \end{Bmatrix} = [H]\{\bar{u}\}, \tag{4}$$

where $\{\bar{u}\} = \{u_0, v_0, w_0, \partial w_0/\partial x, \partial w_0/\partial y\}^{\text{T}}$ are the midplane displacements in the x, y and z directions, and the rotations of the yz and xz planes due to bending, and

$$[H] = \begin{bmatrix} 1 & 0 & 0 & -z & 0 \\ 0 & 1 & 0 & 0 & -z \\ 0 & 0 & 1 & 0 & 0 \end{bmatrix}. \tag{5}$$

The strains associated with the displacement field in Eq. (4) are given by

$$\begin{Bmatrix} \varepsilon_1 \\ \varepsilon_2 \\ \varepsilon_6 \end{Bmatrix} = \begin{Bmatrix} \frac{\partial u_0}{\partial x} \\ \frac{\partial v_0}{\partial y} \\ \frac{\partial u_0}{\partial y} + \frac{\partial v_0}{\partial x} \end{Bmatrix} - z \begin{Bmatrix} \frac{\partial^2 w_0}{\partial x^2} \\ \frac{\partial^2 w_0}{\partial y^2} \\ 2\frac{\partial^2 w_0}{\partial x \partial y} \end{Bmatrix}. \tag{6}$$

3.2. Constitutive relationships

Quasi-static and plane stress formulations are assumed in the present analysis. Thus, the constitutive relationship for the FGM lamina in the principal material coordinates of the lamina, taking into account the piezoelectric effects, is given as follows:

$$\begin{Bmatrix} \sigma_1 \\ \sigma_2 \\ \sigma_6 \end{Bmatrix} = \begin{bmatrix} c_{11} & c_{12} & 0 \\ c_{12} & c_{22} & 0 \\ 0 & 0 & c_{66} \end{bmatrix} \begin{Bmatrix} \varepsilon_1 \\ \varepsilon_2 \\ \varepsilon_6 \end{Bmatrix} - \begin{bmatrix} 0 & 0 & e_{31} \\ 0 & 0 & e_{32} \\ 0 & 0 & 0 \end{bmatrix} \begin{Bmatrix} E_1 \\ E_2 \\ E_3 \end{Bmatrix}, \tag{7}$$

$$\begin{Bmatrix} D_1 \\ D_2 \\ D_3 \end{Bmatrix} = \begin{bmatrix} 0 & 0 & 0 \\ 0 & 0 & 0 \\ e_{31} & e_{32} & 0 \end{bmatrix} \begin{Bmatrix} \varepsilon_1 \\ \varepsilon_2 \\ \varepsilon_6 \end{Bmatrix} + \begin{bmatrix} k_{11} & 0 & 0 \\ 0 & k_{22} & 0 \\ 0 & 0 & k_{33} \end{bmatrix} \begin{Bmatrix} E_1 \\ E_2 \\ E_3 \end{Bmatrix}. \tag{8}$$

Here $E_i = -\Phi_{,i}$ and Φ is the electric potential, $\{\sigma\}$, $\{\varepsilon\}$, $\{E\}$ and $\{D\}$ are the stress, strain, electric field and the electric displacements respectively. $[c]$, $[e]$ and $[k]$ are accordingly the elastic constants, the piezoelectric stress constants and the dielectric permittivity coefficients for a constant elastic strain. For an FGM plate of uniform thickness, the relevant functionally properties of the plate are assumed to vary through the thickness of the plate. The variation of the elastic constants is assumed to be in terms of a simple power law distribution given as

$$c_{ij}(z) = \left(c_{ij}^{\mathrm{T}} - c_{ij}^{\mathrm{A}}\right)\left(\frac{2z+h}{2h}\right)^{n} + c_{ij}^{\mathrm{A}}, \tag{9}$$

where c_{ij}^{T} and c_{ij}^{A} are the corresponding elastic properties of the Ti–6A1–4V and aluminum oxide, n is the volume fraction exponent, and h is the thickness of the plate. The piezoelectric stress constants can be obtained by using the piezoelectric strain and elastic constants as follows:

$$\begin{bmatrix} 0 & 0 & 0 \\ 0 & 0 & 0 \\ e_{31} & e_{32} & 0 \end{bmatrix} = \begin{bmatrix} 0 & 0 & 0 \\ 0 & 0 & 0 \\ d_{31} & d_{32} & 0 \end{bmatrix} \begin{bmatrix} c_{11} & c_{12} & 0 \\ c_{12} & c_{22} & 0 \\ 0 & 0 & c_{66} \end{bmatrix}. \tag{10}$$

3.3. Variational form of the equations of motion

The potential energy H stored in a lamina comprises the various components of the elastic strain energy, the piezoelectric energy and the electrical energy, and is given by (Tiersten, 1969).

$$H\left(\varepsilon_{ij}, E_i\right) = \tfrac{1}{2} c_{ijkl}\varepsilon_{ij}\varepsilon_{kl} - e_{ijk}E_i\varepsilon_{jk} - \tfrac{1}{2}k_{ij}E_iE_j. \tag{11}$$

Thus, the variational form of the equations of motion for the plate can be written, using Hamilton's principle, as

$$\delta\int_{t_0}^{t_1}\int_v\left[\frac{1}{2}\rho\dot{u}_i\dot{u}_i - H\left(\varepsilon_{ij},E_i\right)\right]\mathrm{d}v\,\mathrm{d}t + \int_{t_0}^{t_1}\int_v f_{\mathrm{b}i}\,\delta u_i\,\mathrm{d}v\,\mathrm{d}t + \int_{t_0}^{t_1} f_{\mathrm{c}i}\,\delta u_i\,\mathrm{d}t + \int_{t_0}^{t_1}\int_{\mathrm{s}}\left(f_{\mathrm{s}i}\,\delta u_i + q\,\delta\phi\right)\mathrm{d}s\,\mathrm{d}t = 0 \tag{12}$$

or

$$\int_{t_0}^{t_1}\int_v\left(-\rho\ddot{u}_i\,\delta u_i - \sigma_{ij}\,\delta\varepsilon_{ij} + D_i\,\delta E_i\right)\mathrm{d}v\,\mathrm{d}t + \int_{t_0}^{t_1}\int_v f_{\mathrm{b}i}\,\delta u_i\,\mathrm{d}v\,\mathrm{d}t + \int_{t_0}^{t_1} f_{\mathrm{c}i}\,\delta u_i\,\mathrm{d}t + \int_{t_0}^{t_1}\int_{\mathrm{s}}\left(f_{\mathrm{s}i}\,\delta u_i + q\,\delta\phi\right)\mathrm{d}s\,\mathrm{d}t = 0. \tag{13}$$

Here, t_0 and t_1 describe two arbitrary time values, δ is the variational operator, v and s denote the volume and surface of the solid respectively. The symbol q is the surface charge, $f_{\mathrm{b}i}$, $f_{\mathrm{c}i}$ and $f_{\mathrm{s}i}$ represent the body force, concentrated load and specified traction respectively. The symbol ρ is the density of the plate which varies according to the relationship,

$$\rho(z) = (\rho_T - \rho_{\mathrm{A}})\left(\frac{2z+h}{2h}\right)^n + \rho_{\mathrm{A}}, \tag{14}$$

where ρ_T and ρ_{A} are the densities of Ti–6A1–4V and aluminum oxide, respectively, and

$$D_i = -\frac{\partial H}{\partial E_i} = e_{ijk}\varepsilon_{jk} + k_{ij}E_j, \tag{15}$$

$$\sigma_{ij} = \frac{\partial H}{\partial \varepsilon_{ij}} = c_{ijkl}\varepsilon_{kl} - e_{kij}E_k. \tag{16}$$

4. Finite element model

The displacements and electric potential can be defined in terms of nodal variables as follows:

$$\{u\} = [H][N_u]\{u^{\mathrm{e}}\}, \tag{17}$$

$$\{\phi\} = \left[N_\phi\right]\{\phi^{\mathrm{e}}\}, \tag{18}$$

where $\{u^{\mathrm{e}}\}$ and $\{\phi^{\mathrm{e}}\}$ are the generalized nodal displacements and the nodal electric potentials respectively. $[N_u]$ and $[N_\phi]$ are the shape function matrices and

$$[N_u] = [[N_{u1}][N_{u2}][N_{u3}][N_{u4}]] \tag{19}$$

and

$$[N_{ui}] = \begin{bmatrix} \psi_i & 0 & 0 & 0 & 0 \\ 0 & \psi_i & 0 & 0 & 0 \\ 0 & 0 & g_{i1} & g_{i2} & g_{i3} \\ 0 & 0 & \frac{\partial g_{i1}}{\partial x} & \frac{\partial g_{i2}}{\partial x} & \frac{\partial g_{i3}}{\partial x} \\ 0 & 0 & \frac{\partial g_{i1}}{\partial y} & \frac{\partial g_{i2}}{\partial y} & \frac{\partial g_{i3}}{\partial y} \end{bmatrix} \qquad i = 1,2,3,4. \tag{20}$$

Here, ψ_i are the linear interpolation functions and g_{ij} are the non-conforming Hermite cubic interpolation functions (Reddy, 1997).

The infinitesimal engineering strains associated with the displacements are given by

$$\{\varepsilon\} = [B_u]\{u^e\}, \tag{21}$$

where

$$[B_u] = [[B_{u1}][B_{u2}][B_{u3}][B_{u4}]] = [A_u] - z[C_u] \tag{22}$$

and

$$[B_{ui}] = [A_{ui}] - z[C_{ui}] \quad i = 1,2,3,4, \tag{23}$$

$$[A_{ui}] = \begin{bmatrix} \frac{\partial \psi_i}{\partial x} & 0 & 0 & 0 & 0 \\ 0 & \frac{\partial \psi_i}{\partial y} & 0 & 0 & 0 \\ \frac{\partial \psi_i}{\partial y} & \frac{\partial \psi_i}{\partial x} & 0 & 0 & 0 \end{bmatrix}, \tag{24}$$

$$[C_{ui}] = \begin{bmatrix} 0 & 0 & \frac{\partial^2 g_{i1}}{\partial x^2} & \frac{\partial^2 g_{i2}}{\partial x^2} & \frac{\partial^2 g_{i3}}{\partial x^2} \\ 0 & 0 & \frac{\partial^2 g_{i1}}{\partial y^2} & \frac{\partial^2 g_{i2}}{\partial y^2} & \frac{\partial^2 g_{i3}}{\partial y^2} \\ 0 & 0 & 2\frac{\partial^2 g_{i1}}{\partial x \partial y} & 2\frac{\partial^2 g_{i2}}{\partial x \partial y} & 2\frac{\partial^2 g_{i3}}{\partial x \partial y} \end{bmatrix}. \tag{25}$$

The electric field vector $\{E\}$ is defined in terms of nodal variables as

$$\{E\} = -\nabla\phi = -\left[B_\phi\right]\{\phi^e\}, \tag{26}$$

where

$$\left[B_\phi\right] = \nabla\left[N_\phi\right]. \tag{27}$$

Substituting Eqs. (15)–(17), (21) and (26) into Eq. (13) and assembling the element equations yields

$$[M_{uu}]\{\ddot{u}\} + [K_{uu}]\{u\} + \left[K_{u\phi}\right]\{\phi\} = \{F_m\}, \tag{28}$$

$$\left[K_{\phi u}\right]\{u\} - \left[K_{\phi\phi}\right]\{\phi\} = \left\{F_q\right\}. \tag{29}$$

The matrices and vectors are given by

$$[M_{uu}] = \sum_{\text{elem}}\sum_{K=1}^{NL}\int_{-1}^{1}\int_{-1}^{1}[N_u]^T[I][N_u]|J|\,d\xi\,d\eta, \tag{30}$$

$$\begin{aligned}[K_{uu}] &= \int_v [B_u]^T[C]\left[B_u\right]dv \\ &= \sum_{\text{elem}}\sum_{K=1}^{NL}\int_{-1}^{1}\int_{-1}^{1}\left([A_u]^T[A][A_u] - [A_u]^T[B][C_u] - [C_u]^T[B][A_u] + [C_u]^T[Q]\left[C_u\right]\right)|J|\,d\xi\,d\eta,\end{aligned} \tag{31}$$

$$\begin{aligned}\left[K_{u\phi}\right] &= \int_v [B_u]^T\left[e\right]^T\left[B_\phi\right]dv \\ &= \sum_{\text{elem}}\sum_{K=1}^{NL}\left(z_{K+1} - z_K\right)\int_{-1}^{1}\int_{-1}^{1}\left([A_u]^T\left[e\right]^T\left[B_\phi\right] - \frac{1}{2}(z_{K+1} + z_K)[C_u]^T\left[e\right]^T\left[B_\phi\right]\right)|J|\,d\xi\,d\eta,\end{aligned} \tag{32}$$

$$\begin{aligned}\left[K_{\phi u}\right] &= \int_v \left[B_\phi\right]^{\mathrm{T}}[e][B_u]\,\mathrm{d}v \\ &= \sum_{\text{elem}}\sum_{K=1}^{NL}\left(z_{K+1}-z_K\right)\int_{-1}^{1}\int_{-1}^{1}\left(\left[B_\phi\right]^{\mathrm{T}}[e][A_u]-\frac{1}{2}\left(z_{K+1}+z_K\right)\left[B_\phi\right]^{\mathrm{T}}[e]\left[C_u\right]\right)|J|\,\mathrm{d}\xi\,\mathrm{d}\eta,\end{aligned} \tag{33}$$

$$\left[K_{\phi\phi}\right] = \int_v \left[B_\phi\right]^{\mathrm{T}}[k]\left[B_\phi\right]\mathrm{d}v = \sum_{\text{elem}}\sum_{K=1}^{NL}(z_{K+1}-z_K)\int_{-1}^{1}\int_{-1}^{1}\left[B_\phi\right]^{\mathrm{T}}[k]\left[B_\phi\right]|J|\,\mathrm{d}\xi\,\mathrm{d}\eta, \tag{34}$$

$$\{F_{\mathrm{m}}\} = \int_v [N]^{\mathrm{T}}[H]^{\mathrm{T}}\{f_{\mathrm{b}}\}\,\mathrm{d}v + \int_{s_f}[N]^{\mathrm{T}}[H]^{\mathrm{T}}\{f_{\mathrm{s}}\}\,\mathrm{d}s + [N]^{\mathrm{T}}[H]^{\mathrm{T}}\{f_{\mathrm{c}}\}, \tag{35}$$

$$\left\{F_{\mathrm{q}}^{\mathrm{e}}\right\} = \int_{s_{\mathrm{q}}}\left[N_\phi\right]^{\mathrm{T}}\{q\}\,\mathrm{d}s, \tag{36}$$

where

$$[I] = \int_{z_K}^{z_{K+1}}\left((\rho_T-\rho_{\mathrm{A}})\left(\frac{2z+h}{2h}\right)^n[H]^{\mathrm{T}}[H]+\rho_T[H]^{\mathrm{T}}[H]\right)\mathrm{d}z, \tag{37}$$

$$[A,B,Q] = \int_{z_K}^{z_{K+1}}\left(\left([C]^{\mathrm{T}}-[C]^{\mathrm{A}}\right)\left(\frac{2z+h}{2h}\right)^n\left(1,z,z^2\right)+[C]^{\mathrm{A}}\left(1,z,z^2\right)\right)\mathrm{d}z. \tag{38}$$

Substituting Eq. (29) into Eq. (28), we obtain

$$[M_{uu}]\{\ddot{u}\}+\left([K_{uu}]+\left[K_{u\phi}\right]\left[K_{\phi\phi}\right]^{-1}\left[K_{\phi u}\right]\right)\{u\} = \{F_{\mathrm{m}}\}+\left[K_{u\phi}\right]\left[K_{\phi\phi}\right]^{-1}\left\{F_{\mathrm{q}}\right\}. \tag{39}$$

For the sensor layer, the applied charge $\left\{F_{\mathrm{q}}\right\}$ is zero and the converse piezoelectric effect is assumed negligible. Using Eq. (29), the sensor output is

$$\{\phi\}_{\mathrm{s}} = \left[K_{\phi\phi}\right]_{\mathrm{s}}^{-1}\left[K_{\phi u}\right]_{\mathrm{s}}\{u\}_{\mathrm{s}}, \tag{40}$$

and the sensor charge due to deformation from Eq. (29) is

$$\left\{F_{\mathrm{q}}\right\}_{\mathrm{s}} = \left[K_{\phi u}\right]_{\mathrm{s}}\{u\}_{\mathrm{s}}, \tag{41}$$

where the subscript s denotes the sensors. The control law on $\{\phi\}_{\mathrm{a}}$ is implemented as

$$\{\phi\}_{\mathrm{a}} = G\{\dot{\phi}\}_{\mathrm{s}}, \tag{42}$$

where G is the feedback gain and subscript a denotes the actuators. Substituting Eqs. (42) and (40) into Eq. (29) yields

$$\left\{F_{\mathrm{q}}\right\}_{\mathrm{a}} = \left[K_{\phi u}\right]_{\mathrm{a}}\{u\}_{\mathrm{a}} - G\left[K_{\phi\phi}\right]_{\mathrm{a}}\left[K_{\phi\phi}\right]_{\mathrm{s}}^{-1}\left[K_{\phi u}\right]_{\mathrm{s}}\{\dot{u}\}_{\mathrm{s}}. \tag{43}$$

Substituting Eqs. (41) and (43) into Eq. (39) and rearranging

$$[M_{uu}]\{\ddot{u}\}+[C_{\mathrm{d}}]\{\dot{u}\}+[K_{uu}]\{u\} = \{F_{\mathrm{m}}\}, \tag{44}$$

where $[C_{\mathrm{d}}]$ is the active damping matrix

$$[C_{\mathrm{d}}] = G\left[K_{u\phi}\right]_{\mathrm{a}}\left[K_{\phi\phi}\right]_{\mathrm{s}}^{-1}\left[K_{\phi u}\right]_{\mathrm{s}}. \tag{45}$$

Considering the structural damping effects, Eq. (44) can be rewritten as

$$[M_{uu}]\{\ddot{u}\} + ([C_s] + [C_d])\{\dot{u}\} + [K_{uu}]\{u\} = \{F_m\}, \tag{46}$$

where the damping matrix $[C_s]$ is defined as

$$[C_s] = a[M_{uu}] + b[K_{uu}], \tag{47}$$

where a and b are Rayleigh's coefficients.

5. Results and discussion

To ensure the accuracy of the proposed finite element model, deflection and natural frequency results are calculated for simply supported FGM plates with different values of volume fraction power law exponent n and compared with the results of Praveen and Reddy (1998) and Bishop (1979) as shown in Tables 1 and 2.

Table 1
Variation of non-dimensional center deflection, $\bar{w}$, with the power-law exponent n for simply supported FGM plates

Power-law exponent, n	Present	Praveen and Reddy (1998)
0	0.0847	0.0841
0.2	0.0957	0.0951
0.5	0.1082	0.1075
1.0	0.1211	0.1187
2.0	0.1320	0.1285
∞	0.1820	0.1755

Table 2
Natural frequency ω (Hz) for simply supported FGM plates for the two special cases of isotropy

Mode no.	$n = 0$		$n = 2000$	
	Present	Bishop (1979)	Present	Bishop (1979)
1	144.66	145.04	268.92	271.23
2	360.53	362.61	669.40	678.06
3	360.53	362.61	669.40	678.06
4	569.89	580.18	1052.49	1084.90
5	720.57	725.22	1338.52	1356.10
6	720.57	725.22	1338.52	1356.10
7	919.74	942.79	1695.23	1763.00
8	919.74	942.79	1695.23	1763.00
9	1225.72	1233.00	2280.95	2305.40
10	1225.72	1233.00	2280.98	2305.40

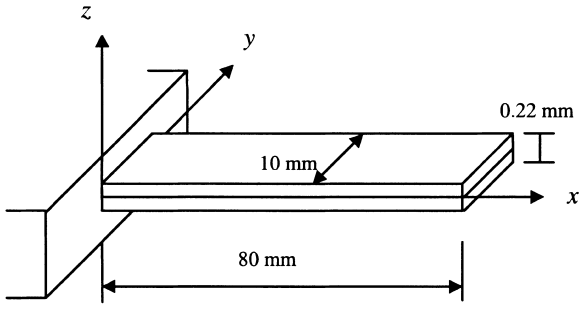

Fig. 2. Piezoelectric KYNAR cantilever beam.

Table 3
Material properties of piezoelectric materials

	KYNAR (Koconis, et al. 1994)	G-1195N (Lam and Ng, 1999)
Elastic modulus E (N/m^2)	6.85×10^9	63×10^9
Poison's ratio v	0.29	0.3
Density ρ (kg/m^3)	–	7600
Piezoelectric constant d_{31} (m/V)	23.0×10^{-12}	254×10^{-12}
Piezoelectric constant d_{32} (m/V)	4.6×10^{-12}	254×10^{-12}
Dielectric coefficients k_{33} (F/m)	–	15×10^{-9}

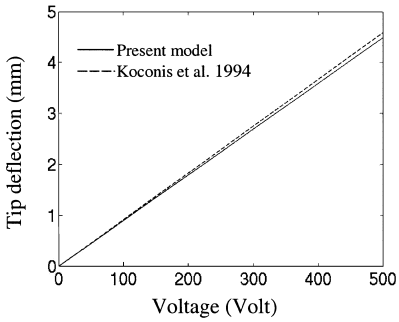

Fig. 3. Tip deflection of the piezoelectric KYNAR cantilever beam versus the input voltage.

It is observed that the present results agree well with those in the literature. Subsequently, a cantilever beam consisting of two layers of KYNAR piezoelectric films, as shown in Fig. 2, is considered. The material properties are listed in Table 3. The effects of applied voltage on the tip deflection are studied and compared with the results obtained by Koconis et al. (1994) (Fig. 3). As can been seen, the results obtained by the present model are in good agreement with the results presented in Koconis et al. (1994).

Having validated the model to a certain extent, static and dynamic studies on an FGM plate with integrated piezoelectric sensor and actuator layers are presented in the tabular and graphical forms. The model under consideration is a cantilevered FGM plate consisting of combined Ti–6A1–4V and aluminum oxide material constituents with different mixing ratios. Fig. 4 show the variation of the volume fraction of Ti–6A1–4V through the plate thickness. G-1195N piezoelectric films bond both the top and bottom surfaces of the FGM plate as shown in Fig. 1. The plate is square with both length and width set at 0.4 m. It is

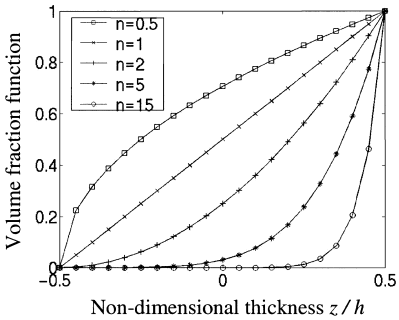

Fig. 4. Variation of the volume fraction function $V_T = (z/h + 0.5)^n$ with the non-dimensional thickness.

Table 4
Materials constants of the constituent materials of the FGM plate

Material constants	Aluminum oxide			Ti–6A1–4V		
	E (N/m^2)	v	ρ (kg/m^3)	E (N/m^2)	v	ρ (kg/m^3)
P_0	349.55×10^9	0.2600	3750	122.56×10^9	0.2884	4429
P_{-1}	0	0	0	0	0	0
P_1	-3.853×10^{-4}	0	0	-4.586×10^{-4}	1.121×10^{-4}	0
P_2	4.027×10^{-7}	0	0	0	0	0
P_3	-1.673×10^{-10}	0	0	0	0	0
P	3.2024×10^{11}	0.2600	3750	1.0570×10^{11}	0.2981	4429

of thickness 5 mm, and each G-1195N piezoelectric layer is of thickness 0.1 mm. The material properties for G-1195N piezoelectric layer and the FGM plate are given in Tables 3 and 4, respectively. The properties of the FGM plate are temperature dependent and are evaluated at a temperature of 300 K. For the following static and dynamic analyses, 64 (8×8) elements are used to model the plate. Unless otherwise specified, all subsequent analyses are based on the model as shown in Fig. 1.

5.1. Static analysis

For deflection or shape control, the top and bottom piezoelectric layers are used as actuators. The top layer is polarized in the direction of the applied voltage and the bottom layer is polarized in the opposite direction of the applied voltage. The cantilevered FGM plate is originally exposed to a uniformly distributed load of 100 N/m^2 and thus has an initial deflection as shown in Fig. 5. The effect of constituent volume fraction $V_T = (z/h + 0.5)^n$ on the deflection is studied by varying the volume fraction of Ti–6A1–4V. This is carried out by varying the value of the power law exponent n. For example, $n = 0$ implies the FGM plate consists only of Ti–6A1–4V. As n increases, the volume fraction of Ti–6A1–4V is decreased, as shown in Fig. 3. When n tends to ∞, the FGM plate almost totally consists of aluminum oxide. It is shown that with the increase of n, the deflection of the FGM plate is decreased. To control the plate deflection, equal-amplitude active voltages of opposite sign are applied across the top and the bottom piezoelectric layers, through the thickness. Fig. 6 show the centerline deflection of a cantilevered FGM plate for various values of the power law exponent n under actuator voltage $V = 40$ V. It is clear from Figs. 5 and 6, that just by adjusting the actuator voltages, one can control shape as well as the position of the maximum deflection point.

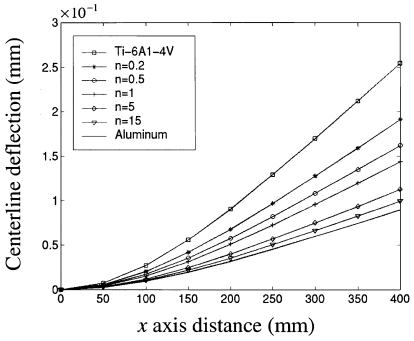

Fig. 5. Centerline deflection of the FGM plate (CFFF) under uniformly distributed load of 100 N/m^2 and actuator voltage $V = 0$ V.

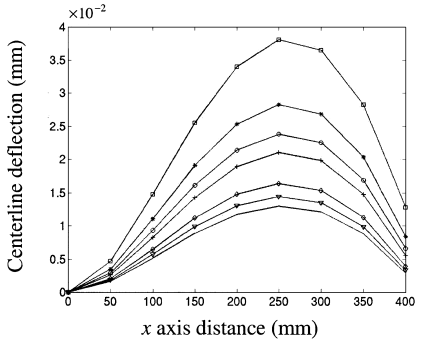

Fig. 6. Centerline deflection of the FGM plate (CFFF) under uniformly distributed load 100 N/m^2 and actuator voltage $V = 40$ V.

5.2. Vibration analysis

The initial ten natural frequencies of the FGM plate as a function of the volume fraction power law exponent n are depicted in Tables 5–7 for various boundary conditions. The dimensions of the FGM plate are the same as that shown in Fig. 1. Three sets of boundary conditions were considered: a cantilevered (CFFF) plate, a simply supported plate (SSSS) plate and a fully clamped (CCCC) plate. Tables 5–7 show

Table 5
Variation of the natural frequencies (Hz) with the power law exponent n for a cantilevered (CFFF) FGM plates with integrated sensor and actuator layers

Mode no.	$n = 0$	$n = 0.2$	$n = 0.5$	$n = 1$	$n = 5$	$n = 15$	$n = 100$	$n = 1000$
1	25.58	29.87	32.84	35.33	40.97	43.97	46.12	46.55
2	62.75	73.67	81.20	87.52	101.85	109.48	114.93	116.00
3	157.20	183.97	202.52	218.04	252.99	271.62	284.96	287.60
4	200.19	233.88	257.28	276.89	321.15	344.76	361.66	365.00
5	228.22	267.51	294.67	317.43	368.76	396.11	415.68	419.55
6	397.58	465.95	513.23	552.85	642.19	689.79	723.85	730.59
7	452.26	528.29	581.31	625.49	723.86	776.40	814.19	821.68
8	472.76	553.15	608.91	655.54	760.22	816.05	856.08	864.00
9	522.91	611.27	672.78	724.11	838.70	899.87	943.83	952.54
10	677.28	792.64	872.64	939.57	1089.95	1170.15	1227.64	1239.02

Table 6
Variation of the natural frequencies (Hz) with the power law exponent n for a simply supported (SSSS) FGM plates with integrated sensor and actuator layers

Mode no.	$n = 0$	$n = 0.2$	$n = 0.5$	$n = 1$	$n = 5$	$n = 15$	$n = 100$	$n = 1000$
1	144.25	168.74	185.45	198.92	230.46	247.30	259.35	261.73
2	359.00	420.66	462.47	495.62	573.82	615.58	645.55	651.49
3	359.00	420.66	462.47	495.62	573.82	615.58	645.55	651.49
4	564.10	665.01	731.12	778.94	902.04	967.78	1014.94	1024.28
5	717.80	841.26	925.45	993.11	1148.12	1231.00	1290.78	1302.64
6	717.80	841.26	925.45	993.11	1148.12	1231.00	1290.78	1302.64
7	908.25	1073.70	1180.93	1255.98	1453.32	1558.77	1634.65	1649.70
8	908.25	1073.70	1180.93	1255.98	1453.32	1558.77	1634.65	1649.70
9	1223.14	1432.16	1576.91	1697.15	1958.17	2097.91	2199.46	2219.67
10	1223.14	1432.16	1576.94	1697.15	1958.17	2097.93	2199.47	2219.68

Table 7
Variation of the natural frequencies (Hz) with the power law exponent n for a fully clamped (CCCC) FGM plates with integrated sensor and actuator layers

Mode no.	$n = 0$	$n = 0.2$	$n = 0.5$	$n = 1$	$n = 5$	$n = 15$	$n = 100$	$n = 1000$
1	262.53	306.42	337.45	363.00	420.26	450.85	472.79	477.14
2	533.83	623.47	687.16	739.30	855.25	917.21	961.79	970.64
3	533.83	623.47	687.16	739.30	855.25	917.21	961.79	970.64
4	774.20	904.40	999.44	1075.32	1243.98	1334.10	1398.98	1411.85
5	957.32	1119.16	1233.99	1327.94	1534.21	1644.53	1724.30	1740.15
6	963.04	1125.80	1241.01	1335.47	1542.96	1653.93	1734.16	1750.09
7	1172.70	1370.83	1516.60	1632.04	1886.53	2022.62	2120.87	2140.36
8	1172.70	1370.83	1516.60	1632.04	1886.53	2022.62	2120.87	2140.36
9	1535.81	1797.55	1981.96	2133.47	2460.92	2636.29	2763.82	2789.22
10	1535.81	1797.55	1981.96	2133.47	2460.92	2636.29	2763.82	2789.22

that the natural frequencies increase with increases in the volume fraction power law exponent n for all the three types of boundary conditions considered here.

For the vibration control, the top piezoelectric layer is used as an integrated actuator and the bottom layer as an integrated sensor, as shown in Fig. 1. The constant velocity feedback control algorithm described earlier is used to control or suppress the vibration of the FGM plate. To simplify the vibration analysis, the modal superposition algorithm is used and first six modes are considered in this modal space analysis. An initial modal damping for each of the modes is assumed to be 0.8%. A unit of force is imposed at point A of the FGM plate (Fig. 1) in the vertical direction and is subsequently removed to generate motion from the initial displacement. The transient response of the FGM plate is analyzed by using the Newmark-β direct integration technique and the parameters γ and β are taken to be 0.5 and 0.25, respectively. All the calculations for transient response are performed with a time step of 0.001 s.

Figs. 7–10 show the decay envelopes of the transient response of point A (Fig. 1) of the FGM plate at various values of the power law exponent n for feedback gain, ranging from 0 to 10^{-1}. The effect of the power-law exponent n on the transient response is similar to that of static analysis in that the vibration amplitude decreases as the power-law exponent n increases. When gain $G = 0$, the transient response still attenuates with time due to structural damping, (Fig. 7). With the introduction of feedback gain, the attenuation of the amplitude of vibration increases considerably. With a gain of $G = 0.1$, the vibration amplitude almost attenuates to almost zero as shown in Fig. 10. Fig. 11 presents the piezoelectric sensor voltage response for a predominantly aluminum oxide plate (i.e. power law exponent $n = \infty$) for various gain values of $G = 10^{-3}$, 10^{-2}, 5×10^{-2} and 10^{-1}. For these various gain values, the results show that peak

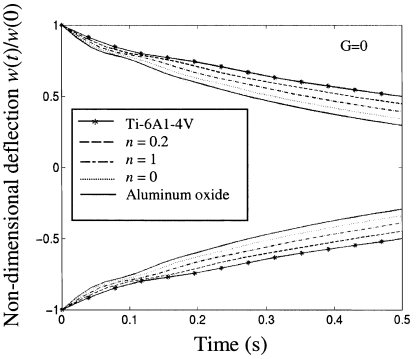

Fig. 7. A plot of decay envelopes showing the variation of the displacements at the tip of the cantilever plate (see point A, Fig. 1) for a gain of 0.

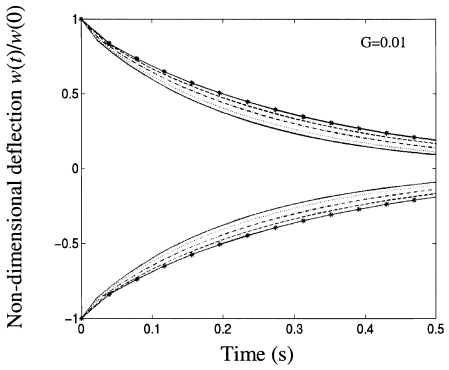

Fig. 8. A plot of decay envelopes showing the variation of the displacements at the tip of the cantilever plate (see point A, Fig. 1) for a gain of 0.01.

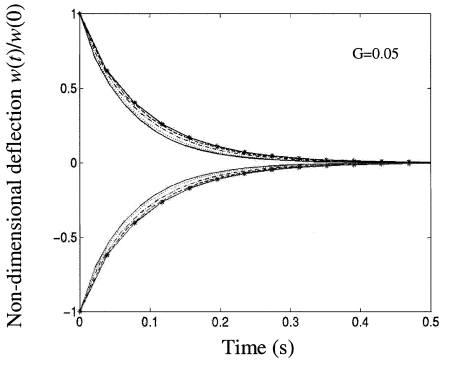

Fig. 9. A plot of decay envelopes showing the variation of the displacements at the tip of the cantilever plate (see point A, Fig. 1) for a gain of 0.05.

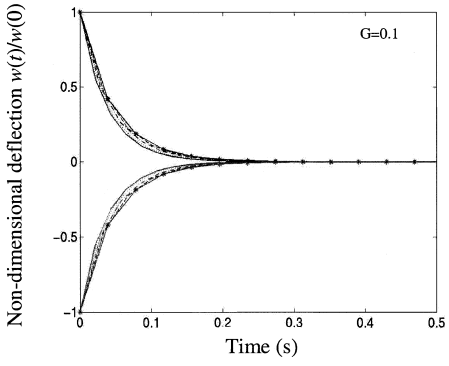

Fig. 10. A plot of decay envelopes showing the variation of the displacements at the tip of the cantilever plate (see point A, Fig. 1) for a gain of 0.1.

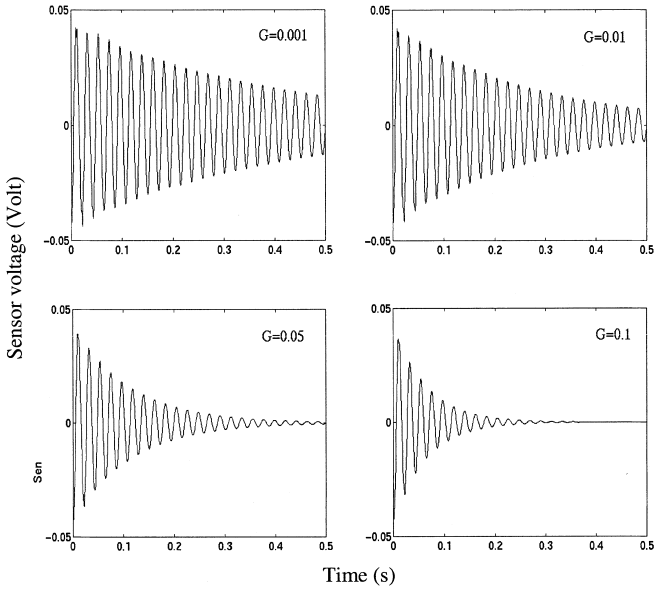

Fig. 11. Plots of piezoelectric sensor response for a cantilever aluminum oxide plate ($n = \infty$) for various gain values, G.

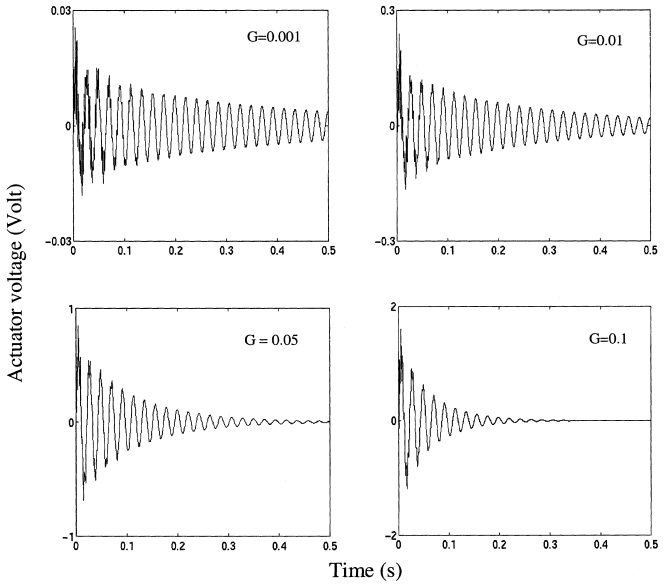

Fig. 12. Plots of piezoelectric actuator response for a cantilever aluminum oxide plate ($n = \infty$) for various gain values, G.

values do not vary and approach the static value due to the initial static deflection. It is also observed that with the increase of the gain, the sensor voltage response attenuates substantially faster. In Fig. 12, the corresponding piezoelectric actuator responses are presented. The actuator voltages increase as the gain values increase with the largest actuator voltage of 1.5 volt occurring at the initial time when gain $G = 0.1$. It should be noted that the gain could not be increased indefinitely as piezoelectric materials have inherent breakdown voltages.

6. Conclusion

An efficient finite element model is presented for carrying out the shape and vibration control of the FGM plates using integrated piezoelectric sensor/actuator layers. The formulation is based on the CLPT, but can be easily extended to higher order laminated plate theories. The properties of the FGM plate are functionally graded in the thickness direction according to a volume fraction power law distribution. Static and dynamic analyses were carried out on the FGM plates for various boundary conditions clearly showing the effects of the constituent volume fraction on the FGM plate responses. For vibration control, a constant velocity control algorithm is applied in a closed loop system to provide active feedback control of the FGM plates. The dynamic response shows that the vibration amplitude of the FGM plate attenuates at very high rates for appropriate gain values, thus demonstrating the effectiveness of the present control algorithm for the vibration control of the FGM plates.

References

Allik, H., Hughes, T.J.R., 1970. Finite element method for piezoelectric vibration. International Journal for Numerical Methods in Numerical Methods in Engineering 2, 151–157.

Bishop, R.E.D., 1979. The Mechanics of Vibration. Cambridge University Press, New York.

Chandrashekhare, K., Tenneti, R., 1995. Thermally induced vibration suppression of laminated plates with piezoelectric sensors and actuators. Smart Materials and Structures 4, 281–290.

Crawley, E.F., Luis, J., 1987. Use of piezoelectric actuators as elements of intelligent structures. AIAA Journal 25, 1373–1385.

Heyliger, P., Pei, K.C., Saravanos, D., 1996. Layerwise mechanics and finite element model for laminated piezoelectric shells. AIAA Journal 34, 2353–2360.

Hwang, W.S., Park, H.C., Hwang, W.B., 1993. Vibration control of laminated plate with piezoelectric sensors and actuators: finite element formulation and model analysis. Journal of Intelligent Material Systems and Structures 4, 317–329.

Koconis, D.B., Kollar, L.P., Springer, G.S., 1994. Shape control of composite plates and shells with embedded actuators I: voltages specified. Journal of Composite Materials 28, 415–458.

Lam, K.Y., Ng, T.Y., 1999. Active control of composite plates with integrated piezoelectric sensors and actuators under various dynamic loading conditions. Smart Materials and Structures 8, 223–237.

Lammering, R., 1991. Application of finite shell element for composite containing piezo-electric polymers in vibration control. Computers and Structures 41, 1101–1109.

Lee, C.K., O'Sullivan, T.C., Chiang, W.W., 1991. Piezoelectric strain sensor and actuator designs for active vibration control. Proceedings of the 32nd AIAA/ASME/ASCE/AHS Structures, Structural Dynamics and Materials Conference, Washington DC, AIAA Paper 91, p. 1064.

Obata, Y., Noda, N., 1996. Optimum material design for functionally gradient material plate. Archive of Applied Mechanics 66, 581–589.

Plump, J.M., Hubbard, J.E., Bailey, T., 1987. Nonlinear control of a distributed system: simulation and experimental results. Journal of Dynamic Systems, Measurement and Control 109, 133–139.

Praveen, G.N., Reddy, J.N., 1998. Nonlinear transitent thermoelastic analysis of functionally graded ceramic–metal plates. International Journal of Solids and Structures 35, 4457–4476.

Reddy, J.N., 1987. A generalization of two-dimensional theories of laminated composite plates. Communication in Applied Numerical Methods 3, 173.

Reddy, J.N., 1997. Mechanics of Laminated Plates: Theory and Analysis. CRC Press, Boca Raton, FL.

Robbins, D.H., Reddy, J.N., 1991. Analysis of piezoelectrically actuated beams using a layer-wise displacement theory. Computers and Structures 41, 265–279.

Tiersten, H.F., 1969. Linear Piezoelectric Plate Vibrations. Plenum Press, New York.

Touloukian, Y.S., 1967. Thermophysical Properties of High Temperature Solid Materials. Macmillian, New York.

Tzou, H.S., Tseng, C.I., 1990. Distributed piezoelectric sensor/actuator design for dynamic measurement/control of distributed parameter systems: a piezoelectric finite element approach. Journal of Sound and Vibration 138, 17–34.

Williamson, R.L., Rabin, B.H., Drake, J.T., 1993. Finite element analysis of thermal residual stresses at graded ceramic–metal interfaces, part I: model description and geometric effects. Journal of Applied Physics 74, 1310–1320.

Yamanouchi, M., Hirai, T., Shiota, I., 1990. Proceedings of the First International Symposium on Functionally Gradient Materials, Japan.